

Crystal Structure and Stoichiometric Composition of Potassium-Intercalated Tetracene

Craig I. Hiley, Kenneth K. Inglis, Marco Zanella, Jiliang Zhang, Troy D. Manning, Matthew S. Dyer, Tilen Knaflić, Denis Arčon, Frédéric Blanc, Kosmas Prassides, and Matthew J. Rosseinsky*

Cite This: *Inorg. Chem.* 2020, 59, 12545–12551

Read Online

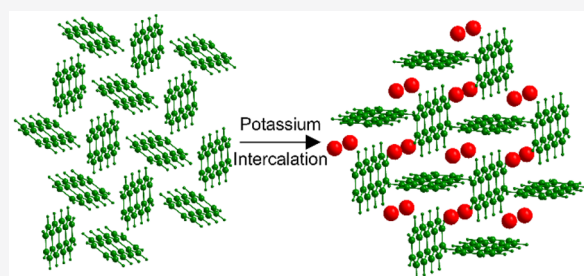
ACCESS |

Metrics & More

Article Recommendations

Supporting Information

ABSTRACT: The products of the solid-state reactions between potassium metal and tetracene (K:Tetracene, 1:1, 1.5:1, and 2:1) are fully structurally characterized. Synchrotron X-ray powder diffraction shows that only K₂Tetracene forms under the reaction conditions studied, with unreacted tetracene always present for $x < 2$. Diffraction and ¹³C MAS NMR show that K₂Tetracene has a crystal structure that is analogous to that of K₂Pentacene, but with the cations ordered on two sites because of the influence of the length of the hydrocarbon on possible cation positions. K₂Tetracene is a nonmagnetic insulator, thus further questioning the nature of reported superconductivity in this class of materials.



INTRODUCTION

Since K_xPicene ($2.6 \leq x \leq 3.3$) was reported to be superconducting with a critical temperature T_c of 18 K,¹ similar phenomena in several other alkali metal-intercalated polyacenes have been claimed,^{2–4} leading to comparisons to the intensively studied alkali metal-doped fullerenes.^{5–7} However, poor reproducibility, miniscule shielding fractions (typically <1%), and a lack of structural or chemical understanding of the alkali metal–polyacene products have led some to question whether the reported superconductivity arises from the purported bulk phase or trace impurities.^{8,9} Preparation and characterization of phase-pure crystalline materials has proven problematic due to the complex reactivity of polyacenes under reducing conditions and the air-sensitivity of the products. As a result, no structural information from the alkali metal–intercalated polyacene materials was available until the reliable syntheses and crystal structures of K₂Pentacene,¹⁰ K₂Picene,¹⁰ CsPhenanthrene,¹¹ Cs₂Phenanthrene,¹¹ and K₂Rubrene¹² were recently reported. All (with the exception of CsPhenanthrene) contain only polyacene dianions, with no unpaired electrons, and an array of magnetic and spectroscopic data show that these phases are insulating with no evidence of metallicity or superconductivity being observed.

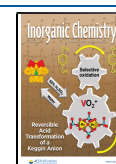
Pentacene and picene are isomers (C₂₂H₁₄) consisting of five fused rings in a linear or zigzag fashion, respectively (Figure S1). K₂Pentacene and K₂Picene were both prepared by direct solid-state reactions of the mild reductant KH with the appropriate (phen)acene.¹⁰ The crystal structures show that both the pentacene and picene anions retain the layered herringbone packing motif found in the structures of pristine

(phen)acenes, but the intermolecular angle, ω , increases from 53° to 58° in the pristine materials to ~90° in the intercalates. This reorientation creates a column of voids between molecules which can be occupied by K⁺ ions, allowing maximum contact with the electron-rich π systems of the molecular anions while also minimizing intermolecular $\pi \cdots \pi$ interactions. In K₂Pentacene, two K ions are disordered over four sites, each of which corresponds to points where the rings are fused by non-hydrogen-bearing carbons, and thus, the aligned pentacene molecules are at their narrowest. In K₂Picene, the situation is complicated by picene orientational disorder which leads to poorly defined K positions within the pocket dictated by the local environment arising from the picene configuration.

Despite the mild reduction conditions, K₂Pentacene was found by powder synchrotron X-ray diffraction (SXRD) to contain a secondary phase with very similar structural parameters to the main phase (there is <0.1% difference between the refined cell volumes of the two phases). The subtlety of the difference between these phases made it impossible to resolve whether the secondary phase is a consequence of nonstoichiometry (i.e., K_{2± δ} Pentacene) or a change in molecular structure. Acenes become progressively more reactive as the chain length increases, and pentacene has

Received: June 3, 2020

Published: August 11, 2020



been shown to undergo thermolysis under inert conditions at temperatures of ~ 300 °C.¹³ Tetracene ($C_{18}H_{12}$) is an analogue of pentacene, consisting of four linearly fused aromatic rings. Tetracene has a highest occupied molecular orbital (HOMO) to lowest unoccupied molecular orbital (LUMO) gap small enough for it to be considered an organic semiconductor (3.0 eV),¹⁴ while being $\sim 20\%$ larger than the HOMO–LUMO gap of pentacene (2.3 eV),¹⁵ making tetracene less reactive^{16,17} and less susceptible to attack by reducing agents. In the solid state, pristine tetracene adopts a herringbone arrangement¹⁸ with a crystal structure analogous to that of pentacene. Reports^{19,20} of KTetracene and K_2 Tetracene samples show powder SXRD patterns which closely resemble that of K_2 Pentacene, though crystal structures have not been presented and it is unclear how K ions are distributed within the pockets of the herringbone structure of the smaller acene. The study of KTetracene was interesting since it would represent the first example of a polyacene salt to contain singly charged anions within a herringbone structure commonly adopted by larger acenes. Herein, we present synthetic attempts to prepare and characterize K_x Tetracene ($1 \leq x \leq 2$) phases. Contrary to previous reports,^{19,20} K_2 Tetracene was found to be the only binary salt of K and tetracene in this compositional range. The phase purity of the prepared samples enable us to report the crystal structure and electronic characterization of this phase.

EXPERIMENTAL DETAILS

Synthesis. K metal and tetracene in the appropriate ratio (total mass ~ 50 mg) were ground together using a pestle and mortar at room temperature in an Ar-filled glovebox (H_2O and O_2 levels < 0.1 ppm). After ~ 30 min of grinding, the metal was completely consumed and the characteristic red color of tetracene was absent, yielding a fine dark-brown ($x < 2$) or black ($x = 2$) powder. The powder was then pelletized, sealed in an evacuated glass tube (pressure $< 10^{-4}$ mbar), and annealed at 140 °C (413 K) for 24 h. Sample pellets were then reground and stored in an Ar-filled glovebox. It should be noted that for samples where $x < 2$ (which were found to contain unreacted tetracene), a second pelletization–annealing step was attempted which, however, did not result in detectable further tetracene consumption (Figure S2).

Chemical Characterization, Structural Solution, and Refinement. Powder XRD and SXRD data were collected at room temperature in transmission mode from 0.7 mm borosilicate capillaries. Laboratory XRD data were used as for initial assessment (Figure S3) and were collected from a Bruker-AXS D8 Advance diffractometer with a fine-focus Mo– $K\alpha$ source ($\lambda = 0.71073$ Å). SXRD data used for structural solution and refinement were collected at Beamline I11 at the Diamond Light Source, U.K. ($\lambda = 0.82608(1)$ Å) using Mythen PSD detectors.

Refinement of the K_2 Tetracene structure was carried out using TOPAS Academic v5,²¹ over the range $2 \leq 2\theta \leq 40$. The pattern could be indexed to a monoclinic cell analogous to that of K_2 Pentacene, but with a lattice parameter c (which is effectively parallel to the long axis of the acene molecule) $\sim 15\%$ shorter; a Le Bail fit shows that this accounts for all peaks in the SXRD pattern (Figure S4). As such, a starting model based on that of K_2 Pentacene was produced,¹⁰ whereby a herringbone array of tetracene molecules was constructed and three K atoms were added to each pocket within the array, with sites corresponding to the narrowest point of the tetracene molecular ions. A Rietveld refinement of the structure was then carried out. In order to minimize the number of refined variables, rigid bodies with centers fixed around inversion centers in the unit cell were used to model the two crystallographically distinct tetracene molecular ions. The rigid body was allowed to rotate freely and was constrained to have a single, refined C–C bond distance of 1.4538(6) Å. C–H bonds were fixed to 1.1 Å. The occupancies of the K atoms were allowed to refine, and the occupancy of the K atom

aligned with the center of the tetracene molecules was close to zero. Removing the atom from this site improved the overall fit, while the occupancies of the other two K sites remained close to 1 (0.946(9) and 0.964(9) for K1 and K2 sites, respectively) upon refinement, so subsequent refinements were fixed at 1. Attempts to refine the C thermal parameter yielded negative (i.e., unphysical) results (likely a consequence of approximating the molecule as an idealized rigid body), so C and H isotropic thermal parameters were fixed at a reasonable value ($B_{eq} = 0.8$ Å²) with minimal effect on the reliability factor (0.04% discrepancy in R_{wp} compared to the model with freely refined C thermal parameters). The K atoms' isotropic thermal displacement parameters were constrained to have a single value and allowed to refine freely. An anisotropic peak broadening model by Stephens²² was used to fit peak shapes in both the Le Bail and Rietveld fits. This yielded a final fit (Figure 1a, Figure S5) with 44 directly refined parameters, with 12 arising from the background function, 3 instrumental parameters (axial divergence, scaling factor, and zero error), 4 lattice parameters, 15 atomic parameters (comprising of K fractional coordinates, isotropic thermal parameters

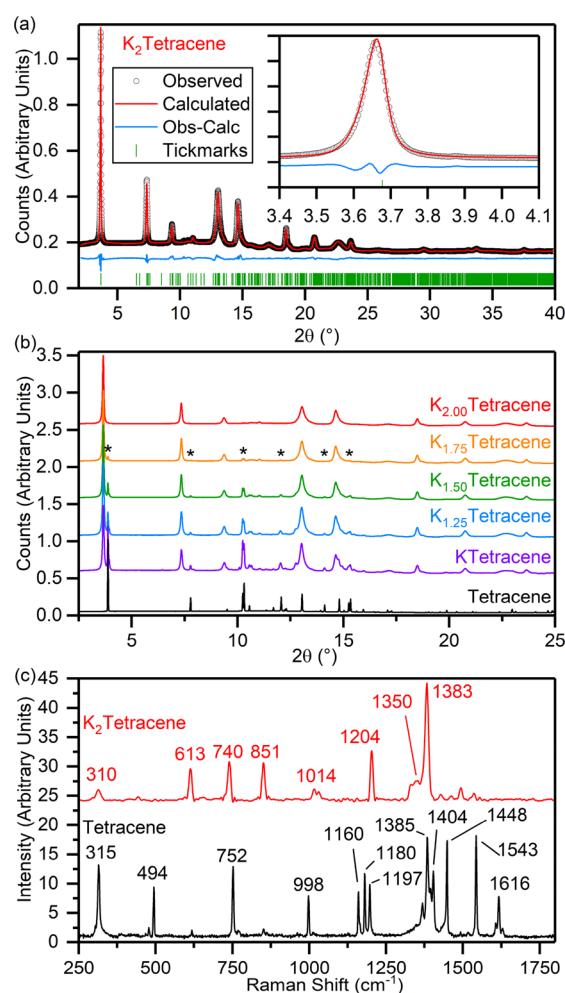


Figure 1. (a) Results of a Rietveld refinement of K_2 Tetracene structure to SXRD data ($R_{wp} = 2.96\%$; $R_{exp} = 0.47\%$, $P2_1/c$, $a = 7.2599(4)$ Å, $b = 7.2749(4)$ Å, $c = 25.756(1)$ Å, $\beta = 91.78(1)^\circ$). Inset shows the (002) diffraction peak; no unreacted tetracene or other secondary phases are present. (b) SXRD patterns from K_x Tetracene ($1 \leq x \leq 2$) samples compared to pristine tetracene ($\lambda = 0.82608(1)$ Å). Patterns offset by 0.5 arbitrary units for clarity. Asterisks (*) indicate positions of tetracene (“Type 1” polymorph) Bragg peaks observed in samples $x \leq 1.75$. (c) Raman spectra of pristine tetracene and K_2 Tetracene (excitation laser $\lambda = 785$ nm).

for C and K, rotational vectors for two rigid bodies, and the refined C—C bond length), and 10 peak shape parameters.

The ^{13}C solid-state NMR experiment was performed on a commercial 9.4 T Bruker DSX NMR spectrometer using a 4 mm HXY triple-resonance probe (in double resonance). The data were recorded with cross-polarization (CP) under magic angle spinning (MAS) at 14 kHz. ^1H pulses and SPINAL-64²³ heteronuclear decoupling during ^{13}C detection were obtained at a radio frequency (rf) field amplitude of 83 kHz. For the CP step, the ^{13}C rf field was set to 50 kHz, and a ramped rf field was applied on protons and matched to obtain optimal signals at approximately 60 kHz. The CP contact time was set to 2 ms. The ^{13}C spectrum was referenced to the tertiary ^{13}C resonance of adamantane at 29.45 ppm, corresponding to TMS at 0 ppm.²⁴ The sample was packed in the Ar glovebox using a Kel-F high-resolution MAS insert and then was placed in a zirconia rotor with a Kel-F cap.

ICP-OES measurements were collected from samples of $\text{K}_2\text{Tetracene}$ dissolved in 25 mL of dilute nitric acid. Sample measurements were performed utilizing a Spectro Ciros ICP-OES radial view instrument.

Raman spectroscopy was collected from samples sealed in glass capillaries using a Renishaw inVia Raman Spectrometer with an excitation laser wavelength of 785 nm.

DFT Calculations. Non-spin-polarized periodic DFT calculations were performed using VASP²⁵ and CASTEP.²⁶ The experimentally refined crystal structure of $\text{K}_2\text{Tetracene}$ was taken as a starting point, and the cell and atomic positions were optimized in VASP using the optB86b-vdW functional²⁷ to include the effects of van der Waals interactions. A plane-wave cutoff energy of 520 eV was used, with a $7 \times 7 \times 2$ Γ -point centered k -point grid and a force threshold of 0.001 eV \AA^{-1} . The outer-shell electrons of all species and the 3s and 3p electrons of K were treated as valence electrons, with core-electrons treated using the projected augmented wave (PAW) method.²⁸ The structure optimized in VASP was then used to calculate NMR parameters in CASTEP using the GIPAW method.²⁹ For these calculations the PBE functional³⁰ was used, with a plane-wave cutoff energy of 600 eV and a $7 \times 7 \times 2$ Γ -point centered k -point grid. Ultrasoft pseudopotentials were used in CASTEP for the same core electrons as in the VASP PAW calculations. Computed values of the isotropic component of the shielding tensor, σ_{iso} , were converted to predicted experimental shifts, δ_{iso} , for ^{13}C NMR using the formula $\delta_{\text{iso}} = 171 - 1.02\sigma_{\text{iso}}$.³¹

Electronic and Magnetic Characterization. For the EPR measurements, a powder sample with the nominal composition ' $\text{K}_{1.50}\text{Tetracene}$ ' was sealed under a dynamic vacuum in a standard Suprasil quartz tube (outer diameter ~ 4 mm). The continuous-wave X-band EPR experiments were performed on a home-built spectrometer equipped with a Varian E-101 microwave bridge, a Varian TEM104 dual cavity resonator, an Oxford Instruments ESR900 cryostat, and an Oxford Instruments ITC503 temperature controller. The temperature stability was better than ± 0.05 K at all temperatures. The microwave power was set to 1 mW, whereas the amplitude of the modulation field was 0.07 mT. The EPR spectra were measured on cooling.

SQUID magnetometry data were collected from samples contained within silica ampules using a Quantum Design MPMS XL-7 SQUID magnetometer. A modified Curie–Weiss Law of the form $\chi = (C/(T - \theta)) + K$ yielded values of $C = 0.00394(3)$ $\text{cm}^3 \text{K mol}^{-1}$, $\theta = -5(4)$ K, and $K = 2(1) \times 10^{-3}$ $\text{cm}^3 \text{mol}^{-1}$.

RESULTS AND DISCUSSION

Samples with nominal composition $\text{K}_x\text{Tetracene}$ ($1 \leq x \leq 2$) were prepared by solid-state reaction of K metal and tetracene using a protocol inspired by previous synthetic procedures;^{19,20} see the Experimental Section for more information. SXRD of the resulting samples (Figure 1b) reveals Bragg peaks for a new phase formed upon K intercalation, as well as unreacted tetracene (when $x < 2$). However, no peaks attributable to

tetracene are seen in the sample for which $x = 2$ (nominally ' $\text{K}_2\text{Tetracene}$ '). Comparison of the Raman spectrum of $\text{K}_2\text{Tetracene}$ with that of pristine tetracene reveals that there are no vibrational modes associated with neutral tetracene (Figure 1c) and that the spectrum is consistent with formation of tetracene²⁻ anions.³² When either pentacene and picene are directly reacted with K metal, there are significant signs of molecular decomposition.¹⁰ However, this is not the case with tetracene, demonstrating its increased stability. Exposure of the material to air rapidly recovers an orange powder, while XRD analysis shows a mixture of KOH and pristine tetracene (Figure S6), indicating that intercalation does not affect the integrity of the tetracene molecule. ICP-OES elemental analysis of $\text{K}_2\text{Tetracene}$ gives a K content of 28.7(2) wt %, which is close to the expected value of 25.5 wt %. Unlike $\text{K}_2\text{Pentacene}$, no crystalline secondary phases are observed for $\text{K}_2\text{Tetracene}$ as all peaks in the powder pattern can be indexed to a monoclinic cell ($P2_1/c$, $a = 7.2599(4)$ \AA , $b = 7.2749(4)$ \AA , $c = 25.756(1)$ \AA , $\beta = 91.78(1)^\circ$). The monoclinic cell is analogous to that of $\text{K}_2\text{Pentacene}$ ¹⁰ (Figure 2a), and thus, an

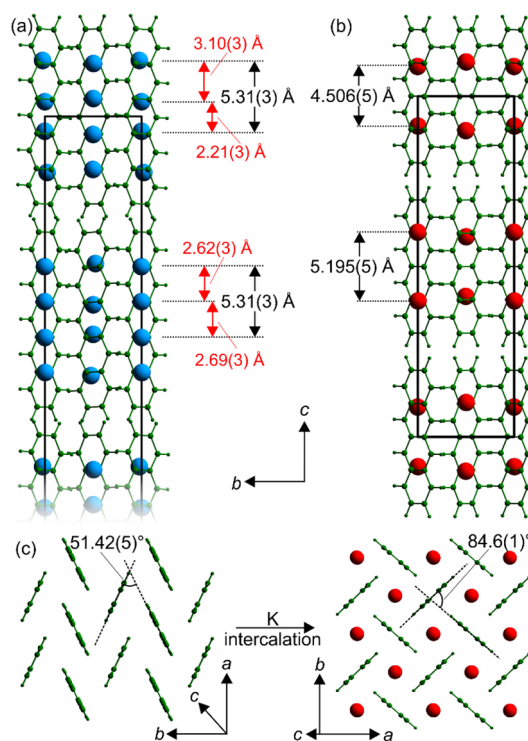


Figure 2. (a, b) Views of $\text{K}_2\text{Pentacene}$ (a) and $\text{K}_2\text{Tetracene}$ (b) along the a axis. Physical and unphysical $\text{K}\cdots\text{K}$ distances are shown in black and red, respectively. Tetracene molecules are shown in green, fully occupied K sites are shown in red, and $\sim 50\%$ occupied sites are shown in blue. Unit cell edges are represented by bold black lines. (c) Herringbone reorientation from tetracene (left) to $\text{K}_2\text{Tetracene}$ (right), with expansion of the layers to accommodate potassium ions.

initial structural model (see Experimental Details, Table S1) for $\text{K}_2\text{Tetracene}$ was constructed based on the $\text{K}_2\text{Pentacene}$ structure, with three cation sites at the fusions of the aromatic rings by analogy with the four sites observed to be partially occupied in $\text{K}_2\text{Pentacene}$. Occupancies of the three K sites were initially set to 0.667, but rapidly diverged, with the K sites at the extremes of the channel refining to close to 1 and the site aligned with the center of the molecule having an occupancy of close to zero. Therefore, this cation site was removed in the

final refinement and the occupancy of the other two K sites was fixed to 1 (Figure 2b, further details of the refinement are given in the Experimental Section). A Rietveld refinement based on this model yields a good fit ($R_{wp} = 2.96\%$) to the SXRD pattern (Figure 1a), comparable in quality to that obtained from a Le Bail fit ($R_{wp} = 2.33\%$, Figure S4). In order to minimize the number of refined parameters the tetracene molecules were described by rigid bodies which were fixed on an inversion center but free to rotate in three dimensions. The rigid bodies contained a single refined C—C bond distance of 1.4538(6) Å, elongated compared to neutral tetracene³³ (mean C—C bond length of 1.40(2) Å) but consistent with increased electron density arising from ion formation and previously noted in other phenacene salts.¹⁰ Rietveld refinements to the SXRD patterns for samples $x < 2$ showed that they consist solely of mixtures of K₂Tetracene and tetracene (Figure S7, Table S2), with no indication of KTetracene phase or of any nonstoichiometric compounds.

Potassium intercalation is shown to expand the herringbone arrangement of the acene (Figure 2c), as in K₂Pentacene and K₂Picene.¹⁰ The intermolecular angle ω increases from $\omega = 51.42(5)^\circ$ in pristine tetracene (ambient stable “Type 1” polymorph³³) to almost perpendicular ($\omega = 86.4(1)^\circ$) in K₂Tetracene, consistent with $\pi \cdots \pi$ repulsion resulting from increased electron density in the polyacene anions. Potassium ions reside in the pockets formed in the expanded herringbone layers, where they have maximum interaction with the aromatic π systems. Within the K-intercalated linear polyacene structures K₂Pentacene and K₂Tetracene, K ions occupy 12-coordinate sites with all nearest neighbor carbon atoms. These are situated parallel to the ternary carbons (i.e., at the points of ring fusion) where the molecules are narrowest, thus minimizing steric hindrance from H atoms (Figure 2a, b). The K—C bond distances in K₂Tetracene range from 2.96(2) to 3.28(1) Å, with a mean bond length of 3.11(3) Å. These are similar to the bond lengths seen in K₂Pentacene (Figure S8). Although the herringbone framework of the K₂Tetracene structure has three sites of sufficient size to accommodate a K ion, only the two at the ends of the pocket are occupied (Figure 2b). This can be rationalized by an examination of the K \cdots K interaction distances; the minimum physical distance between two K cations is ~ 4 Å (determined from KH,³⁴ where the hydride anions effectively occupy interstitial holes in a K cation fcc lattice³⁵). Since nearest neighboring K sites in K₂Pentacene are separated by distances ranging from 2.21(3) to 3.10(3) Å (Figure 2a), neighboring sites cannot be simultaneously occupied. There are four K sites within each pocket (Figure 2a), and there are three possible ways to arrange two ions over these (obeying the rule that no neighboring sites are occupied), leading to a random distribution of K atoms and $\sim 50\%$ occupancy for each site. The same rule that no two neighboring sites are occupied also applies to K₂Tetracene, where the distance between the two occupied K sites is 4.576(6) to 5.118(7) Å and thus precludes a K site at the center of the pocket for the same reasons described for K₂Pentacene. Full occupancy of the two sites in K₂Tetracene leads to a single possible K-arrangement of the correct composition, making this phase the only disorder-free K-intercalated acene known to date.

The lack of disorder is further confirmed by the ¹³C cross-polarization (CP) magic angle spinning (MAS) NMR spectrum of K₂Tetracene (Figure 3), which shows five well-resolved carbon environments of which one is split into two

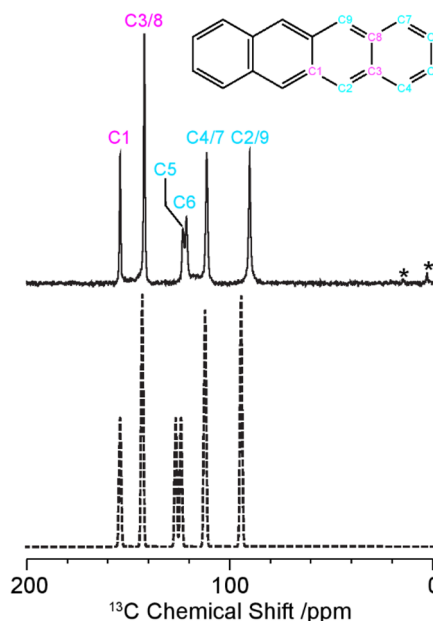


Figure 3. Experimental (full line) and simulated (dotted line) ¹³C solid-state MAS NMR spectra of K₂Tetracene at 9.4 T. The simulated spectrum is based on the chemical shifts predicted from the DFT model with the signal intensity fixed to the number of corresponding carbons. The spectral assignment is given on a molecule of tetracene for simplicity. The similar carbons of the two independent tetracene molecules in K₂Tetracene are not resolved experimentally and differ by a maximum of 0.1 ppm within the predicted shifts (Table S3); these carbons are therefore not labeled for clarity. Quaternary carbons are in purple and CH carbon in light blue. Asterisks (*) denote spinning sidebands arising from ¹³C chemical shift anisotropy.

partially resolved signals at 121.3 and 123.0 ppm (Table S3 and see below). The crystal structure contains two crystallographically distinct tetracene subunits each with 9 C sites (18 C sites in total); they are in almost identical chemical environments with predicted shifts differing by ≤ 0.1 ppm for analogous carbon sites and are, therefore, indistinguishable in this experiment (see below). The ¹³C resonances span a much wider range of chemical shifts (>60 ppm) than the aromatic carbons in tetracene (that all appear within less than 5 ppm around 130 ppm). This is consistent with a range of shielding arising from varied electron density from the tetracene anions and K cations. The structure determined from diffraction data was used as the starting point for periodic density functional theory (DFT) calculations to computationally predict the ¹³C NMR shifts expected from this crystallographic model. The different ¹³C signals in K₂Tetracene are assigned based on the excellent agreement obtained between the experimental data and the predicted ¹³C chemical shieldings (Figure 3, Table S3), ¹³C-edited NMR spectra collected at various CP contact times, and well-established ¹³C chemical shifts in the literature.³⁶ The carbon C5/C6 splitting mentioned above is due to the slight variation in nearest K \cdots C contacts at each end of the molecule (K \cdots C5 = 3.97(1) Å vs K \cdots C6 = 4.06(1) Å), yielding a resolvable ¹³C C5/C6 chemical shift difference of 1.7 ppm that is also well captured by the predicted shifts (2.6 ppm, Table S3). The DFT calculations also predict some splitting for the C2/C9, C3/C8, and C4/C7 carbons due to two slightly different environments; however, the K \cdots C distance differences are smaller in these environments (K \cdots C2 = 3.04(1) Å vs K \cdots C9 = 2.99(1) Å; K \cdots C3 = 3.09(1) Å vs

$K\cdots C8 = 3.11(1) \text{ \AA}$; $K\cdots C4 = 3.03(1) \text{ \AA}$ vs $K\cdots C7 = 3.09(1) \text{ \AA}$), and therefore, induce only very small chemical shift differences (up to 0.4 ppm) which are smaller than the ^{13}C NMR full-widths at half-maximum (0.8 to 1.5 ppm), hindering experimental observation of the splitting. It is also worth pointing out that although NMR spectra collected under CP conditions are not quantitative, the similar CP kinetics expected for carbons of the same type allow C1:C3/8 ratios of 1:2 and C2/9:C4/7:C5:C6 ratios of 1:1:0.5:0.5 to be estimated, further confirming that $\text{K}_2\text{Tetracene}$ is disorder-free.

Magnetic susceptibility measurements as a function of temperature from $\text{K}_2\text{Tetracene}$ in a weak magnetic field ($H = 20 \text{ Oe}$) give a paramagnetic response, and a modified Curie–Weiss fit (details in the Experimental section) yields a molar Curie constant of $0.00394(3) \text{ cm}^3 \text{ K mol}^{-1}$, suggesting 1.04(1)% impurity spins (Figure 4a). No significant difference

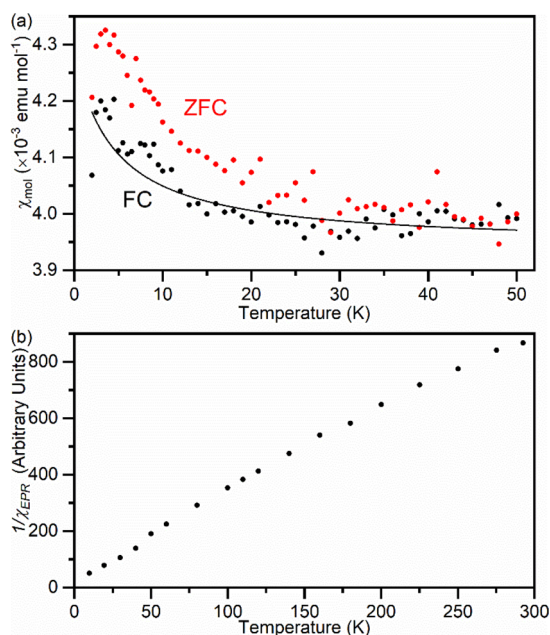


Figure 4. (a) Zero-field-cooled (ZFC, red data points) and field-cooled (FC, black data points) molar magnetic susceptibility of $\text{K}_2\text{Tetracene}$ in a 20 Oe (0.002 T) field with a Curie–Weiss fit to the field-cooled data shown with a solid black line. Parameters for the Curie–Weiss fit are given in the Experimental Section. (b) Inverse X-band EPR susceptibility of the sample with nominal composition $\text{K}_{1.50}\text{Tetracene}$ (XRD analysis shows this consists of $\text{K}_2\text{Tetracene}$ and tetracene in 3:1 ratio).

between the field-cooled and zero-field-cooled data down to 2 K was observed, and there was no evidence for a superconducting transition arising from this material. Similarly, the electron paramagnetic resonance (EPR) signal of a sample (Figure S9a) with nominal composition ' $\text{K}_{1.50}\text{Tetracene}$ ' is very weak, and its calibrated intensity corresponds to localized unpaired spins on $\sim 4\%$ tetracene units. As a function of temperature (Figure 4b) the inverse signal intensity displays simple paramagnetic Curie dependence, while $g = 2.0028$ and the small signal line width of 0.17–0.28 mT are almost independent of temperature (Figure S9b,c). This corroborates the suggestion that the measured EPR signal is indeed due to the small concentration of non-interacting defect spins residing on tetracene molecules and further confirms that in samples where $x < 2$, no phases containing unpaired electrons (such as

KTetracene) are formed in significant quantities. The main phases present contain only tetracene $^{2-}$ ions or neutral tetracene.

CONCLUSIONS

We have explored the binary K–tetracene system and found that under the conditions used in this study the stoichiometric compound $\text{K}_2\text{Tetracene}$ is the only binary phase that can be formed over the range $1 \leq x \leq 2$. Diffraction studies establish that $\text{K}_2\text{Tetracene}$ has a structure analogous to that of $\text{K}_2\text{Pentacene}$, however, with an important difference; in $\text{K}_2\text{Tetracene}$ the cations are not disordered due to there being fewer sites within the structure in which they can reside. This emphasizes the controlling role played by the distances between the candidate cation sites over the ring fusions in determining the occupancy in these intercalated acene structures. The ^{13}C MAS NMR spectrum and agreement with the DFT calculated spectrum indirectly show the presence of two K ions and further validate the lack of disorder in $\text{K}_2\text{Tetracene}$. Raman spectroscopy confirms that the tetracene $^{2-}$ ion forms, and $\text{K}_2\text{Tetracene}$ was found to be in a singlet ground state with no evidence of a superconducting transition. This further questions the nature of reported superconductivity in this class of materials.⁹ The successful use of K metal in these reactions to obtain phase-pure materials with no indication of amorphous secondary phases also demonstrates that, for stable acenes, a direct reaction with K offers a simple and easily controllable route to acene salts. Acene stability declines with increase in the number of rings.

ASSOCIATED CONTENT

Supporting Information

The Supporting Information is available free of charge at <https://pubs.acs.org/doi/10.1021/acs.inorgchem.0c01635>. Underlying data for this article can be accessed at [10.17638/datacat.liverpool.ac.uk/987](https://datacat.liverpool.ac.uk/987).


Additional SXR data and Rietveld fits, crystal structure data and refinement details, K–C bond distances, and additional laboratory PXRD data (PDF)

Accession Codes

CCDC 2006871 contains the supplementary crystallographic data for this paper. These data can be obtained free of charge via www.ccdc.cam.ac.uk/data_request/cif, or by emailing data_request@ccdc.cam.ac.uk, or by contacting The Cambridge Crystallographic Data Centre, 12 Union Road, Cambridge CB2 1EZ, UK; fax: +44 1223 336033.

AUTHOR INFORMATION

Corresponding Author

Matthew J. Rosseinsky – Department of Chemistry, University of Liverpool, Liverpool L7 3NY, United Kingdom;
 orcid.org/0000-0002-1910-2483; Email: m.j.rosseinsky@liverpool.ac.uk

Authors

Craig I. Hiley – Department of Chemistry, University of Liverpool, Liverpool L7 3NY, United Kingdom
 Kenneth K. Inglis – Department of Chemistry, University of Liverpool, Liverpool L7 3NY, United Kingdom
 Marco Zanella – Department of Chemistry, University of Liverpool, Liverpool L7 3NY, United Kingdom

Jiliang Zhang – Department of Chemistry, University of Liverpool, Liverpool L7 3NY, United Kingdom

Troy D. Manning – Department of Chemistry, University of Liverpool, Liverpool L7 3NY, United Kingdom; orcid.org/0000-0002-7624-4306

Matthew S. Dyer – Department of Chemistry, University of Liverpool, Liverpool L7 3NY, United Kingdom; orcid.org/0000-0002-4923-3003

Tilen Knaflič – Jozef Stefan Institute, SI-1000 Ljubljana, Slovenia

Denis Arčon – Jozef Stefan Institute, SI-1000 Ljubljana, Slovenia; Faculty of Mathematics and Physics, University of Ljubljana, SI-1000 Ljubljana, Slovenia; orcid.org/0000-0002-1207-8337

Frédéric Blanc – Department of Chemistry and Stephenson Institute for Renewable Energy, University of Liverpool, Liverpool L7 3NY, United Kingdom; orcid.org/0000-0001-9171-1454

Kosmas Prassides – Department of Materials Science, Graduate School of Engineering, Osaka Prefecture University, Osaka 599-8531, Japan; Advanced Institute for Materials Research (WPI-AIMR), Tohoku University, Aoba-ku, Sendai 980-8577, Japan; orcid.org/0000-0003-4524-3084

Complete contact information is available at:

<https://pubs.acs.org/10.1021/acs.inorgchem.0c01635>

Notes

The authors declare no competing financial interest.

ACKNOWLEDGMENTS

We thank EPSRC for funding under grants EP/K027212/1 and EP/K027255/2 and a studentship to K.K.I. Prof. Laurence Hardwick is thanked for the use of the Renishaw inVia Raman spectrometer. This work was carried out with the support of the Diamond Light Source on Beamline I11. We thank Chiu Tang and Claire Murray for assistance in collecting SXRD data. The financial support of the Slovenian Research Agency under program no. P1-0125 and projects no. J1-9145 and N1-0052 is acknowledged. This work was financially supported by Grants-in-Aid for Scientific Research (JSPS KAKENHI JP17H05139, JP18H04303, JP18K18724, and JP19H04590) by the Ministry of Education, Culture, Sports, Science, and Technology (MEXT), Japan, and by the KAKENHI Specific Support Operation of Osaka Prefecture University.

REFERENCES

- (1) Mitsuhashi, R.; Suzuki, Y.; Yamanari, Y.; Mitamura, H.; Kambe, T.; Ikeda, N.; Okamoto, H.; Fujiwara, A.; Yamaji, M.; Kawasaki, N.; Maniwa, Y.; Kubozono, Y. Superconductivity in alkali-metal-doped picene. *Nature* **2010**, *464* (7285), 76–79.
- (2) Kubozono, Y.; Mitamura, H.; Lee, X.; He, X.; Yamanari, Y.; Takahashi, Y.; Suzuki, Y.; Kaji, Y.; Eguchi, R.; Akaike, K.; Kambe, T.; Okamoto, H.; Fujiwara, A.; Kato, T.; Kosugi, T.; Aoki, H. Metal-intercalated aromatic hydrocarbons: a new class of carbon-based superconductors. *Phys. Chem. Chem. Phys.* **2011**, *13* (37), 16476–16493.
- (3) Wang, X. F.; Liu, R. H.; Gui, Z.; Xie, Y. L.; Yan, Y. J.; Ying, J. J.; Luo, X. G.; Chen, X. H. Superconductivity at 5 K in alkali-metal-doped phenanthrene. *Nat. Commun.* **2011**, *2*, 507.
- (4) Xue, M.; Cao, T.; Wang, D.; Wu, Y.; Yang, H.; Dong, X.; He, J.; Li, F.; Chen, G. F. Superconductivity above 30 K in alkali-metal-doped hydrocarbon. *Sci. Rep.* **2012**, *2*, 389.
- (5) Haddon, R. C.; Hebard, A. F.; Rosseinsky, M. J.; Murphy, D. W.; Duclos, S. J.; Lyons, K. B.; Miller, B.; Rosamilia, J. M.; Fleming, R. M.;

Kortan, A. R.; Glarum, S. H.; Makhija, A. V.; Muller, A. J.; Eick, R. H.; Zahurak, S. M.; Tycko, R.; Dabbagh, G.; Thiel, F. A. Conducting films of C₆₀ and C₇₀ by alkali-metal doping. *Nature* **1991**, *350* (6316), 320–322.

(6) Hebard, A. F.; Rosseinsky, M. J.; Haddon, R. C.; Murphy, D. W.; Glarum, S. H.; Palstra, T. T. M.; Ramirez, A. P.; Kortan, A. R. Superconductivity at 18 K in potassium-doped C₆₀. *Nature* **1991**, *350* (6319), 600–601.

(7) Rosseinsky, M. J.; Ramirez, A. P.; Glarum, S. H.; Murphy, D. W.; Haddon, R. C.; Hebard, A. F.; Palstra, T. T. M.; Kortan, A. R.; Zahurak, S. M.; Makhija, A. V. Superconductivity at 28 K in Rb_xC₆₀. *Phys. Rev. Lett.* **1991**, *66* (21), 2830–2832.

(8) Ruff, A.; Sing, M.; Claessen, R.; Lee, H.; Tomić, M.; Jeschke, H. O.; Valentí, R. Absence of Metallicity in K-doped Picene: Importance of Electronic Correlations. *Phys. Rev. Lett.* **2013**, *110* (21), 216403.

(9) Heguri, S.; Kobayashi, M.; Tanigaki, K. Questioning the existence of superconducting potassium doped phases for aromatic hydrocarbons. *Phys. Rev. B: Condens. Matter Mater. Phys.* **2015**, *92* (1), 014502.

(10) Romero, F. D.; Pitcher, M. J.; Hiley, C. I.; Whitehead, G. F. S.; Kar, S.; Ganin, A. Y.; Antypov, D.; Collins, C.; Dyer, M. S.; Klupp, G.; Colman, R. H.; Prassides, K.; Rosseinsky, M. J. Redox-controlled potassium intercalation into two polyaromatic hydrocarbon solids. *Nat. Chem.* **2017**, *9*, 644.

(11) Takabayashi, Y.; Menelaou, M.; Tamura, H.; Takemori, N.; Koretsune, T.; Štefaničič, A.; Klupp, G.; Buurma, A. J. C.; Nomura, Y.; Arita, R.; Arčon, D.; Rosseinsky, M. J.; Prassides, K. π -electron S = 1/2 quantum spin-liquid state in an ionic polyaromatic hydrocarbon. *Nat. Chem.* **2017**, *9*, 635.

(12) Zhang, J.; Whitehead, G. F.; Manning, T. D.; Stewart, D.; Hiley, C. I.; Pitcher, M. J.; Jansat, S.; Prassides, K.; Rosseinsky, M. J. The reactivity of solid rubrene with potassium: competition between intercalation and molecular decomposition. *J. Am. Chem. Soc.* **2018**, *140* (51), 18162–18172.

(13) Roberson, L. B.; Kowalik, J.; Tolbert, L. M.; Kloc, C.; Zeis, R.; Chi, X.; Fleming, R.; Wilkins, C. Pentacene Disproportionation during Sublimation for Field-Effect Transistors. *J. Am. Chem. Soc.* **2005**, *127* (9), 3069–3075.

(14) Takahashi, T.; Takenobu, T.; Takeya, J.; Iwasa, Y. Ambipolar Light-Emitting Transistors of a Tetracene Single Crystal. *Adv. Funct. Mater.* **2007**, *17* (10), 1623–1628.

(15) Ruiz-Morales, Y. HOMO-LUMO Gap as an Index of Molecular Size and Structure for Polycyclic Aromatic Hydrocarbons (PAHs) and Asphaltenes: A Theoretical Study. *I. J. Phys. Chem. A* **2002**, *106* (46), 11283–11308.

(16) Aihara, J.-I. Reduced HOMO-LUMO Gap as an Index of Kinetic Stability for Polycyclic Aromatic Hydrocarbons. *J. Phys. Chem. A* **1999**, *103* (37), 7487–7495.

(17) Mondal, R.; Tönshoff, C.; Khon, D.; Neckers, D. C.; Bettinger, H. F. Synthesis, Stability, and Photochemistry of Pentacene, Hexacene, and Heptacene: A Matrix Isolation Study. *J. Am. Chem. Soc.* **2009**, *131* (40), 14281–14289.

(18) Desiraju, G. R.; Gavezzotti, A. Crystal structures of polynuclear aromatic hydrocarbons. Classification, rationalization and prediction from molecular structure. *Acta Crystallogr., Sect. B: Struct. Sci.* **1989**, *45* (5), 473–482.

(19) Phan, Q. T. N.; Heguri, S.; Tamura, H.; Nakano, T.; Nozue, Y.; Tanigaki, K. Two different ground states in K-intercalated polyacenes. *Phys. Rev. B: Condens. Matter Mater. Phys.* **2016**, *93* (7), 075130.

(20) Phan, Q. T. N.; Heguri, S.; Tanabe, Y.; Shimotani, H.; Tanigaki, K. Systematic Study of the Electronic States in Electron-Doped Polyacenes. *Eur. J. Inorg. Chem.* **2014**, *2014* (24), 4033–4038.

(21) Coelho, A. A. *Topas-Academic v5*; Coelho Software: 2012.

(22) Stephens, P. Phenomenological model of anisotropic peak broadening in powder diffraction. *J. Appl. Crystallogr.* **1999**, *32* (2), 281–289.

(23) Fung, B. M.; Khitritin, A. K.; Ermolaev, K. An Improved Broadband Decoupling Sequence for Liquid Crystals and Solids. *J. Magn. Reson.* **2000**, *142* (1), 97–101.

- (24) Morcombe, C. R.; Zilm, K. W. Chemical shift referencing in MAS solid state NMR. *J. Magn. Reson.* **2003**, *162* (2), 479–486.
- (25) Kresse, G.; Furthmüller, J. Efficient iterative schemes for ab initio total-energy calculations using a plane-wave basis set. *Phys. Rev. B: Condens. Matter Mater. Phys.* **1996**, *54* (16), 11169–11186.
- (26) Clark, S. J.; Segall, M. D.; Pickard, C. J.; Hasnip, P. J.; Probert, M. I. J.; Refson, K.; Payne, M. C. First principles methods using CASTEP. *Z. Kristallogr. - Cryst. Mater.* **2005**, *220* (5/6), 1.
- (27) Klimeš, J.; Bowler, D. R.; Michaelides, A. Van der Waals density functionals applied to solids. *Phys. Rev. B: Condens. Matter Mater. Phys.* **2011**, *83* (19), 195131.
- (28) Kresse, G.; Joubert, D. From ultrasoft pseudopotentials to the projector augmented-wave method. *Phys. Rev. B: Condens. Matter Mater. Phys.* **1999**, *59* (3), 1758–1775.
- (29) Pickard, C. J.; Mauri, F. All-electron magnetic response with pseudopotentials: NMR chemical shifts. *Phys. Rev. B: Condens. Matter Mater. Phys.* **2001**, *63* (24), 245101.
- (30) Perdew, J. P.; Burke, K.; Ernzerhof, M. Generalized Gradient Approximation Made Simple. *Phys. Rev. Lett.* **1996**, *77* (18), 3865–3868.
- (31) Johnston, J. C.; Iulicci, R. J.; Facelli, J. C.; Fitzgerald, G.; Mueller, K. T. Intermolecular shielding contributions studied by modeling the C13 chemical-shift tensors of organic single crystals with plane waves. *J. Chem. Phys.* **2009**, *131* (14), 144503.
- (32) Sidorov, A. N.; Aleksandrov, I. V.; Bobovich, Y. S. Resonance spectra of spontaneous Raman scattering of negative and positive tetracene ions. *Theor. Exp. Chem.* **1976**, *10* (4), 418–420.
- (33) Holmes, D.; Kumaraswamy, S.; Matzger, A. J.; Vollhardt, K. P. C. On the Nature of Nonplanarity in the [N]Phenylenes. *Chem. - Eur. J.* **1999**, *5* (11), 3399–3412.
- (34) Kuznetsov, V. G.; Shkrabkina, M. M. X-ray diffraction study of NaH and KH at temperatures from 20 to 400°C. *J. Struct. Chem.* **1962**, *3* (5), 532–537.
- (35) Lang, P. F.; Smith, B. C. Ionic radii for Group 1 and Group 2 halide, hydride, fluoride, oxide, sulfide, selenide and telluride crystals. *Dalton Trans.* **2010**, *39* (33), 7786–7791.
- (36) Silverstein, R. M.; Webster, F. X.; Kiemle, D.; Bryce, D. L. *Spectrometric Identification of Organic Compounds*, 8th ed.; Wiley: 2014.